

1-1998


## Dynamic Analysis of Unidirectional Pressure Infiltration of Porous Preforms by Pure Metals

Dhiman K. Biswas  
*Comsys*

Jorge E. Gatica  
*Cleveland State University*

Surendra N. Tewari  
*Cleveland State University*

Follow this and additional works at: [https://engagedscholarship.csuohio.edu/encbe\\_facpub](https://engagedscholarship.csuohio.edu/encbe_facpub)

 Part of the [Materials Science and Engineering Commons](#), and the [Transport Phenomena Commons](#)  
**How does access to this work benefit you? Let us know!**

---

### Original Citation

Biswas, D.K., Gatica, J.E., & Tewari, S.N. (1998). Dynamic Analysis of Unidirectional Pressure Infiltration of Porous Preforms by Pure Metals. *Metallurgical and Materials Transactions A: Physical Metallurgy and Materials Science* 29, 377-385.

### Repository Citation

Biswas, Dhiman K.; Gatica, Jorge E.; and Tewari, Surendra N., "Dynamic Analysis of Unidirectional Pressure Infiltration of Porous Preforms by Pure Metals" (1998). *Chemical & Biomedical Engineering Faculty Publications*. 11.  
[https://engagedscholarship.csuohio.edu/encbe\\_facpub/11](https://engagedscholarship.csuohio.edu/encbe_facpub/11)

This Article is brought to you for free and open access by the Chemical & Biomedical Engineering Department at EngagedScholarship@CSU. It has been accepted for inclusion in Chemical & Biomedical Engineering Faculty Publications by an authorized administrator of EngagedScholarship@CSU. For more information, please contact [library.es@csuohio.edu](mailto:library.es@csuohio.edu).

# Dynamic Analysis of Unidirectional Pressure Infiltration of Porous Preforms by Pure Metals

DHIMAN K. BISWAS, JORGE E. GATICA, and SURENDRA N. TEWARI

Unidirectional pressure infiltration of porous preforms by molten metals is investigated numerically. A phenomenological model to describe fluid flow and transport phenomena during infiltration of fibrous preforms by a metal is formulated. The model describes the dynamics of the infiltration process, the temperature distribution, and solid fraction distribution. The numerical results are compared against classical asymptotic analyses and experimental results. This comparison shows that end effects may become important and render asymptotic results unreliable for realistic samples. Fiber volume fraction and initial temperature appear as the factors most strongly influencing infiltration. Metal superheating affects not only the length of the two-phase zone but also the solid fraction distribution in the two-phase zone. The effect of constant applied pressure, although significant on the infiltration velocity, is almost negligible on the two-phase zone length and on solid fraction distribution. When the initial preform temperature is below the metal melting point, and constant pressure is applied under adiabatic conditions, the flow ceases when sufficient solidification occurs to obstruct it. A comparison with literature experiments proves the model to be an efficient predictive tool in the analysis of infiltration processes for different preform/melt systems.

## I. INTRODUCTION

OVER the past 2 decades, advanced composite materials have progressed from a laboratory curiosity to a production reality. In principle, composites can be constructed of any combination of two or more materials. Metallic composites or metal-matrix composites (MMCs) reinforced with fibers are currently of significant interest. They offer the opportunity to tailor a material with a combination of properties unavailable in any single material, *e.g.*, combining the very high tensile strength and modulus of elasticity of various types of fibers with the low density of a metal such as aluminum, titanium, or magnesium to obtain a composite material with a higher strength-to-density or modulus-to-density ratio than any single known alloy.

Among the several MMC fabrication processes available, the liquid infiltration process referred to as squeeze casting is receiving increasing attention because of its economic feasibility. Liquid metal-matrix infiltration or pressure infiltration, as shown schematically in Figure 1(a), uses pressurized inert gas to force a liquid metal into a preheated porous preform of reinforcement material. Unlike other MMC fabrication methods, pressure infiltration is conducted within the controlled environment of a pressure vessel. This makes it possible to cast complex structures in thin-walled low strength molds. High infiltration pressures can be applied, keeping very low differential pressures between the inside and the outside of the mold, thus reducing the mold required wall thickness and minimizing costs.

For the pressure infiltration process, the pressure gradient, infiltration velocity, temperatures of the preform and superheated melt, and physicochemical properties of the preform are critical variables determining the microstructure of the final composite. Before solidification occurs, the preform permeability is constant and the infiltration velocity is only a weak function of the infiltration length (*cf.* Figure 1(b)). For pure metals, as solidification starts, a two-phase (liquid + solid) region emerges with a time-space varying solid fraction, and the infiltration dynamics become strongly dependent on the infiltration length and solid fraction (*cf.* Figure 1(c)). This two-phase zone is confined between two sharp fronts: a remelting front at the point where the superheated melt enters the two-phase zone and an infiltration front. These two fronts have independent dynamics resulting in a two-phase zone that expands with the infiltration time.

Because of their considerable engineering relevance to MMC fabrication, infiltration processes have been extensively studied, from both theoretical (numerical modeling) and experimental standpoints.<sup>[1-11]</sup> However, given the complexity of the interacting phenomena in this process, several assumptions have been made in most studies involving numerical modeling, or attention has been given only to some specific issues. In this study, a more detailed description and analysis of the existing physical phenomena occurring during pressure infiltration casting are presented.

Nagata and Matsuda<sup>[1]</sup> investigated the infiltration of packed beds with particles sizes varying over a wide range. These authors propose the existence of a critical preform preheating temperature based upon physical constants of the metal and particles, above which the particles must be heated in order to ensure complete infiltration. Martins *et al.*<sup>[2]</sup> formulated a model by considering a bundle of capillary tubes as an analog to the porous compact. This work re-examined the modeling of capillary-induced infiltration kinetics as developed for a capillary-tube-bundle concept.

DHIMAN K. BISWAS, formerly Graduate Student, Department of Chemical Engineering, Cleveland State University, is Software Engineer, Comsys, Information Technology Services, Raleigh, NC 27612. JORGE E. GATICA, Associate Professor, and SURENDRA N. TEWARI, Professor, are with the Department of Chemical Engineering, Cleveland State University, Cleveland, OH 44115-2425.

Manuscript submitted March 26, 1996.

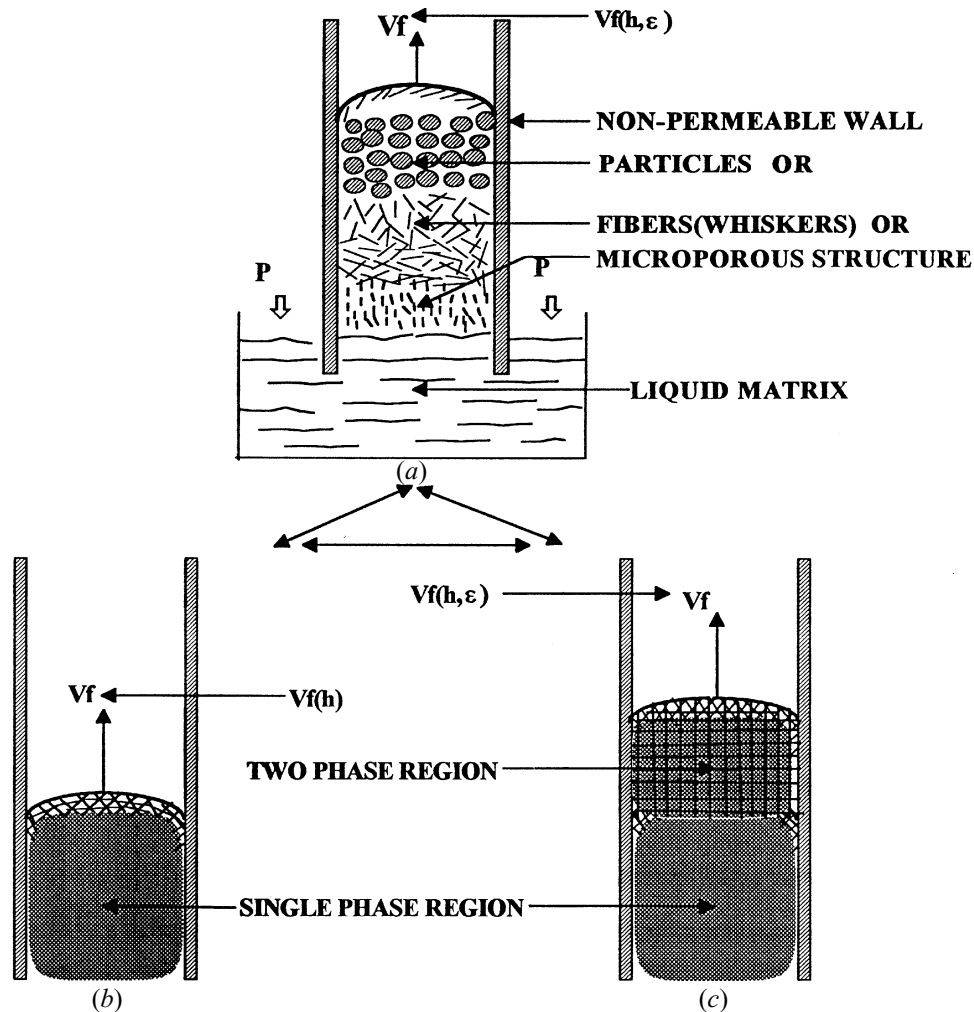


Fig. 1—(a) Schematic of the pressure infiltration process (b) without and (c) with partial solidification.

Girot *et al.*<sup>[3]</sup> presented a numerical analysis of the infiltration of liquid alloys into fibrous preforms. These authors proposed that flow would cease when the metal cools to its liquidus temperature and, therefore, did not account for the release of latent heat of solidification by the metal in their calculations. Mortensen *et al.*<sup>[4]</sup> derived general expressions to describe fluid flow and heat transfer during infiltration of fibrous preforms by a pure metal. Under the conditions of unidirectional infiltration and constant pressure difference, the governing equations were significantly simplified and a solution by a similarity transformation was possible. The same authors also presented experimental results<sup>[5]</sup> for pure aluminum flowing into fibrous alumina preforms to compare with their theory. Mortensen and co-workers also investigated the critical pressure necessary for melt infiltration and the effect of infiltration pressure on the fiber preform deformation. Mortensen and Michaud<sup>[6]</sup> extended the analysis for a binary hypoeutectic alloy. Solidification and mass transport considerations were added. In this model, however, a constant pattern of propagation with flat infiltration and remelting fronts was assumed. Later, Calhoun and Mortensen<sup>[7]</sup> analyzed the morphological stability of the remelting front of a simplified infiltration system (steady-state, unidirectional, adiabatic infiltration with a pure metal) using linear stability analysis. Lacoste *et al.*<sup>[8]</sup> presented a

model for the infiltration of aluminum into a SAFFIL\* pre-

\*SAFFIL is a nominally 3- $\mu\text{m}$ -diameter  $\delta\text{-Al}_2\text{O}_3$  fiber that is chopped and pressed into disk-shaped preforms. SAFFIL is a trademark of ICI Americas, Inc., Wilmington, DE.

form. A one-dimensional (1-D) model was compared with existing analytical solutions. A two-dimensional (2-D) model was formulated and solved as well. The solutions, however, show that 2-D patterns would be restricted to the vicinity of the solidification front for the operating conditions analyzed.

A comprehensive modeling in one and two dimensions was reported recently by Shin<sup>[9]</sup> for the infiltration of pure metals and alloys. This author formulated a detailed model of the process; the commercial computational fluid dynamics package PHOENICS<sup>[12]</sup> was used for the numerical calculations. A very comprehensive analysis was carried out for a typical case study. Comparison with asymptotic analytical results<sup>[5]</sup> revealed minor differences, which the author attributed to the numerical treatment of the source terms. Despite the complexity, the model did not account for remelting phenomena occurring upstream from the infiltration front when superheated melt enters in contact with partially solidified metal. The analysis thus did not investigate the effect of metal superheating on the process. The

study was extended to the infiltration of alloys in one and two dimensions. The results successfully identified some of the phenomena responsible for macrosegregation in composites prepared by alloy infiltration.

Only in very recent works have the dynamics of the infiltration process been addressed. However, emphasis has been given to more specific issues related to the properties of the resulting composite rather than to the infiltration process itself. Thus, for instance, Long *et al.*<sup>[10]</sup> analyzed the formation of noninfiltration defects during liquid metal infiltration of unidirectional continuous fiber arrays. These authors focused on the description of the microscale hydrodynamic phenomena to predict the formation of macro and micro noninfiltration defects in composites. Yamauchi and Nishida,<sup>[11]</sup> on the other hand, concentrated their efforts on very high-pressure (10 to 100 MPa) infiltration experiments, focusing their attention on preform deformation phenomena due to the large pressure gradients.

## II. MODEL EQUATIONS AND ASSUMPTIONS

The analysis of fluid flow and transport phenomena in manufacturing processes is usually based on the transport equations resulting from differential balance laws. The solution to these equations, subject to the pertinent boundary and initial conditions, yields detailed temperature and phase distributions. A detailed knowledge of these fields, together with information about the velocity fields, allows the prediction of global trends and/or effects. When complex structures such as porous media or randomly packed beds are involved, these equations are valid even inside the pores. The geometric complexity of a randomly interconnected porous network prevents any general solution of detailed temperature, solid fraction, and flow fields. Some form of macroscopic balance based on the average over a small volumetric element must be employed.

Even with such a simplification, the description remains of heterogeneous nature (fluid and solid phases). It has been shown,<sup>[13]</sup> however, that a reliable representation of a heterogeneous medium can be achieved *via* a homogeneous model, provided the transport coefficients are suitably chosen. This model, known as pseudohomogeneous, treats the system as a quasicontinuum medium by introducing the concept of effective transport properties. The dimensionless energy balances for the composite (melt and fibers) and preform (inert gas and fibers) are

$$\begin{aligned} \frac{\partial \Phi_c}{\partial t} &= -\nabla \cdot \mathbf{v} \Phi_m + \rho_c \nabla_\theta^2 + S_c \\ \frac{\partial \Phi_p}{\partial t} &= -\nabla \cdot \mathbf{v} \Phi_g + \rho_p \nabla_\theta^2 + S_p \end{aligned} \quad [1]$$

where  $\rho$  is density,  $\theta$  is the dimensionless temperature,  $\Phi$  is the dimensionless enthalpy, and  $\mathbf{v}$  is the velocity vector. The subscripts *c*, *p*, *m*, and *g* signify composite, preform, melt, and gas, respectively.

The flow distribution in unbounded porous media is usually well represented by a linear correlation between the pressure drop and the fluid velocity. This relation is the well-known Darcy's law. The use of such an approximation has been the subject of several analyses and modifications; the details can be found elsewhere.<sup>[14]</sup> For a fluid that obeys

Boussinesq's approximations, and for low infiltration velocities, the momentum equation becomes

$$\frac{1}{\sigma} \frac{1}{\text{Pr}^*} \frac{\partial \mathbf{v}}{\partial t} = -\nabla p - \mathbf{v} + \text{Ra}_T \theta \frac{\mathbf{g}}{|\mathbf{g}|} \quad [2]$$

where  $\text{Pr}^*$  is the Darcy number (or Prandtl for porous media),  $\text{Ra}_T$  is the thermal Rayleigh number,  $\mathbf{g}$  is the gravitational vector, and  $\sigma$  is the fluid to fiber heat capacity ratio. For most situations of interest,<sup>[15]</sup> the Darcy number is much larger than unity ( $\text{Pr}^* \gg 1$ ) and the time dependency can be neglected in the momentum equation. Then, the flow field can be accurately represented by

$$\begin{aligned} 0 &= -\nabla p - \mathbf{v} + \text{Ra}_T \theta \frac{\mathbf{g}}{|\mathbf{g}|} \\ 0 &= \nabla \cdot \mathbf{v} \end{aligned} \quad [3]$$

In developing Eq. [3], solid and fiber phases were assumed stationary, and the difference between solid and liquid metal densities was assumed negligible; *i.e.*, the momentum transfer due to phase change was neglected. The pressure drop was assumed independent of the infiltration front velocity, and the applied pressure was considered high enough for the flow to be slug type.

### A. Initial and Boundary Conditions

To solve the governing equations, Eqs. [1] and [3], one initial condition and four boundary conditions are necessary. In this model for unidirectional infiltration with a constant applied pressure, there is always a period at the beginning of the infiltration process during which high flow velocities are observed. The use of Darcy's law requires a flow with a Reynolds number to be below a critical value. Since the flow is characterized by an initial period of very high flow velocity, which is slowed down as the infiltration takes place, there would be a length the metal must travel before the Reynolds number reaches its critical value. This length, often negligible when compared with the total preform length, is a function of system physical parameters. For instance, Masur *et al.*<sup>[5]</sup> found this length to be approximately 0.3 mm for their experimental conditions. Therefore, the equations will only be applicable after a small section of the preform,  $L_c$ , has been infiltrated. The initial temperature in the melt and preform zones will then be a continuous function, which can be approximated as the analytical solution to the energy balance equation in the preform zone; *i.e.*,

$$\theta(0, x) = \begin{cases} \theta_o & \text{for } x < L_c \\ (\theta_o - \theta_p) \operatorname{erfc}\left(\frac{x}{2\sqrt{\alpha_p t_c}}\right) + \theta_p & \text{for } x \geq L_c \end{cases} \quad [4]$$

where  $t_c$  is the time needed for the melt to travel the critical distance,  $L_c$ , and  $\alpha_p$  is the preform thermal diffusivity. The variables  $\theta_p$  and  $\theta_o$  represent the initial preform and melt dimensionless temperatures, respectively.

Two of the boundary conditions can be formulated at the "infiltration front interface," which separates uninfiltrated preform from infiltrated two-phase zone. Since the infiltration front is tracked *via* a moving grid, no flow will occur through this boundary. Thermal equilibrium at the infiltration front interface establishes

$$\text{and } \left. \begin{aligned} \theta_{L_f^-} &= \theta_{L_f^+} \\ k_c \mathbf{n} \cdot \nabla \theta_{L_f^-} &= k_p \mathbf{n} \cdot \nabla \theta_{L_f^+} \end{aligned} \right\} \text{ at } x=L_f \quad [5]$$

where  $L_f$  is the axial location of the infiltration front,  $\mathbf{n}$  stands for the unitary vector normal to the surface, and  $k_c$  and  $k_p$  are the composite and preform effective thermal conductivities, respectively.

The remaining two boundary conditions, inlet and exit conditions, are assumed as suggested by Danckwerts<sup>[16]</sup> for flow systems; *i.e.*,

$$\text{and } \left. \begin{aligned} \mathbf{n}^- \cdot \mathbf{v} (\Phi_o - \Phi_c) &= \mathbf{n}^+ \cdot \nabla \theta & \text{at } x=0 \\ \mathbf{n}^- \cdot \nabla \theta &= 0 & \text{at } x=1 \end{aligned} \right\} \quad [6]$$

where  $\Phi_o$  and  $\Phi_c$  stand for the superheated metal and composite enthalpies, respectively.

### B. Permeability and Capillary Pressure

For flow perpendicular to the fiber axes, the permeability can be based on the numerical calculations of Sangani and Acrivos,<sup>[17]</sup> as

$$\kappa = \frac{2\sqrt{2} R_f^2}{9(1-\varepsilon)} \left( 1 - 2\sqrt{\frac{1-\varepsilon}{\pi}} \right)^{5/2} \quad [7]$$

where  $R_f$  is the radius of the fibers and  $\varepsilon$  is the void fraction. This equation is valid for void fractions  $1 - m/4 \leq \varepsilon \leq 0.8$ .

For flow parallel to the fiber axes, the permeability can be based on the calculations presented by Drummond and Tahir,<sup>[18]</sup>

$$\kappa = \frac{0.427 R_f^2}{1-\varepsilon} \left[ 1 - \sqrt{\frac{2(1-\varepsilon)}{\pi}} \right]^4 \left[ 1 + 0.473 \sqrt{\frac{\pi - 2(1-\varepsilon)}{2(1-\varepsilon)}} \right] \quad [8]$$

for void fractions  $1 - m/4 \leq \varepsilon \leq 0.5$ .

For infiltration conditions without solidification, the void fraction remains constant and so does the preform permeability. As partial solidification takes place, a void fraction distribution will develop throughout the two-phase zone. Therefore, for solidification conditions, the preform permeability will be a function of space and time, and the infiltration velocity will need to be recalculated. The infiltration velocity can be easily recalculated using the following approach:<sup>[19]</sup>

$$V = -\frac{\langle \kappa \rangle}{\mu_m} \frac{\Delta P}{L_f} \quad [9]$$

where

$$\frac{\langle \kappa \rangle}{\mu_m} = \frac{L_f}{\mu_m \int_0^{L_f} \frac{\mu/\mu_m}{\kappa} dx}$$

Pressure is the only driving force for infiltration to occur. This driving force can be applied externally or by capillary pressure. For wetting systems where capillary pressure is negative, external pressure is not required to initiate infil-

tration. Liquid metals usually do not wet the fibers; therefore, impregnation requires external pressure. Because of the poor wettability and small diameter of modern fibers, the pressure must be large enough to ensure an optimum contact between matrix and fiber. However, very high pressures to avoid inside void can cause fiber breakup. Mortensen and Jin<sup>[20]</sup> showed that the lowest pressure necessary to drive the molten metal into the reinforcement preform can be formulated as a product of the surface area of interface per unit volume of metal matrix and the difference between the interfacial energy of fiber liquid and fiber atmosphere. In other words, this threshold pressure is a physical property that depends on the preform materials, its configuration, and on the infiltrating melt; and it is usually measured experimentally. This critical pressure, nevertheless, is often low enough to enable the assumption of constant surface pressure. For instance, a 1 MPa threshold pressure was found for the infiltration of SAFFIL (alumina) fibers with aluminum.<sup>[6]</sup>

The relation among the total applied pressure  $P_T$ , the capillary pressure,  $\Delta P_\gamma$ , the gas pressure in the preform  $P_g$ , and the pressure differential that drives the flow of the metal into the preform,  $\Delta P$ , can be formulated as

$$\Delta P = P_T - P_g - \Delta P_\gamma \quad [10]$$

Finally, it is worth mentioning here that fabrication of MMCs involves high pressure melt infiltration of a fibrous or porous preform at temperatures higher than the melting point of the metal/alloy. During infiltration, chemical reactions between the preform and the melt may occur, resulting in the formation of a compound layer on the fiber-metal interface. This reaction may or may not be desirable, depending on the properties of the reaction product. The reaction product, *i.e.*, the compound layer, can play a key role in determining mechanical properties of the composites and infiltration dynamics. This subject, although beyond the scope of this article, might be of preponderant relevance for the process under analysis, and the reader is referred to the literature for its analysis.<sup>[25]</sup>

### III. SOLUTION PROCEDURE

The occurrence of solidification during infiltration, *i.e.*, a phase change, can be classified as a moving boundary problem. For this kind of problem, the solution of a differential equation has to satisfy a number of boundary conditions within a prescribed domain, but the boundary has to be determined as a part of the solution because it is not known in advance. Moreover, the position of the boundary is a function of time and space.

Depending on the choice of the dependent variable, two approaches are available for the solution of solid/liquid convection/diffusion phase-change problems.<sup>[9]</sup> In the more general classical method, the temperature is the sole dependent variable, and the energy conservation equations are written separately for the two regions. This is referred to as the temperature-based method. In the second formulation, the enthalpy is used as a dependent variable along with the temperature. This method is called the enthalpy method.<sup>[21-24]</sup>

The differences, as well as advantages and disadvantages, of the temperature- and enthalpy-based formulations

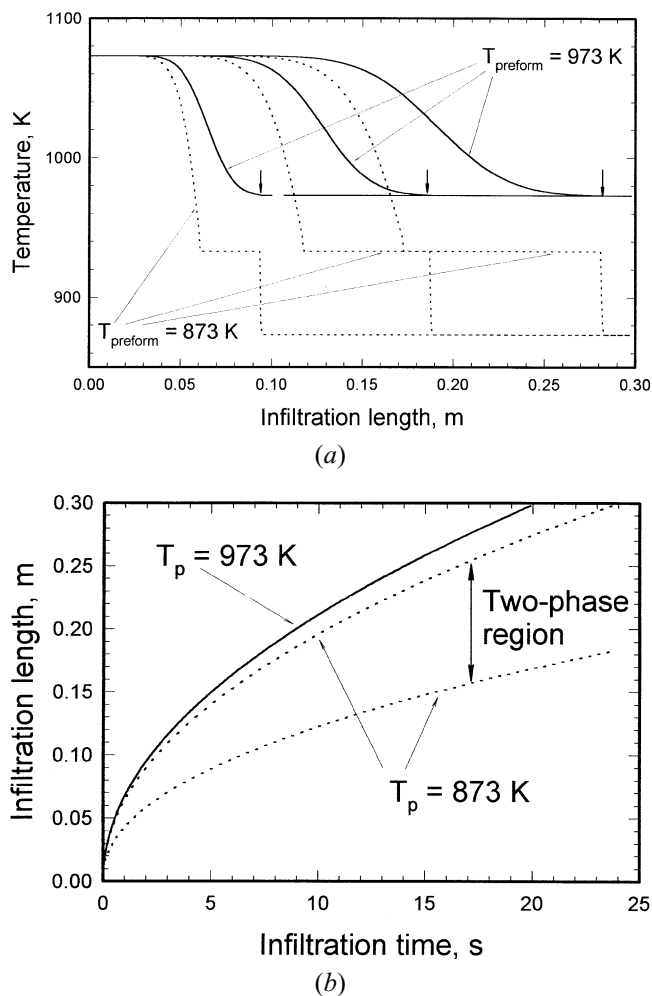


Fig. 2—Infiltration of pure Al into a SAFFIL fiber packed preform, without (solid line) and with (dashed line) solidification: (a) temperature profiles and (b) infiltration dynamics.

are as follows. The temperature-based formulation of the energy equation requires conditions on temperature, velocity, and heat transfer be specified in the vicinity of the solid/liquid phase-change boundary. This causes a difficulty in the application of a fixed-grid numerical solution, as deforming grids or transformed coordinate systems are required to account for the position of the phase-change front. Thus, careful development of software including *ad hoc* features is often necessary. The enthalpy-based formulation, on the other hand, removes the need to satisfy the conditions at the phase-change front. This approach has three advantages: first, fixed-grid numerical solution schemes can be employed; second, physical discontinuities encountered in pure systems and eutectics can be avoided numerically; and third, the enthalpy method can be easily modified to accommodate systems that solidify over a range of temperature and do not exhibit a well-defined solid/liquid interface. The main disadvantage of the enthalpy-based formulation is that the location of the phase-change front cannot be determined exactly. In systems with complicated transport processes close to the solid/liquid interface, this can represent a major problem.<sup>[24]</sup> For 1-D propagation problems, however, the steep temperature profiles developing at solidifying fronts can be efficiently resolved by

using a mapping transformation in a Lagrange formulation, with the front propagation being tracked by an additional equation.<sup>[25]</sup>

Numerical solutions give detailed information, useful in understanding the effect of processing conditions on the microstructure of infiltrated composites. In contrast to the similarity solutions, the numerical analyses are particularly amenable to treating multidimensional (2-D) situations and segregation dynamics (alloys).

To solve the governing equations, Eqs. [1] through [3], the system is discretized, with the maximum number of cells limited by the hypothesis of continuum. The governing equations are applied for each cell; the equations in differences are derived by following a control volume formulation using upstream formulation for the convective terms and central differences for the conduction terms. Three different sets of equations result: the preform side (fibers and inert gas), the composite (preform and melt), and the cell where the infiltration front is located. The incoming and outgoing fluids for the convection term for the cell where the front is located are melt and gas, respectively. The heat conduction takes place on one side of this cell through the composite (fiber and melt) and on the other side through the preform (fiber and gas). Therefore, the rate of energy exchange by conduction at the “front” cell is obtained by one-sided differences, which are used to obtain the thermal gradient for each side. Different thermal conductivities are used for each side. A moving grid line is used to monitor the “filling” of the computational cell where the front is located. The results for temperature and enthalpy are updated after each iteration, while the solid fraction and infiltration velocity are updated only after filling each computational cell. The numerical stability is ensured by selecting the proper number of steps to “fill” a cell (*i.e.*, integration time-step).

#### IV. RESULTS AND DISCUSSION

Figures 2(a) and (b) show typical infiltration results for the infiltration of superheated aluminum into a SAFFIL fiber-packed preform. As the superheated metal (1073 K) infiltrates the preform, it comes in contact with the packing (fibers) at a lower temperature, and therefore, the melt temperature decreases along the preform. As the infiltration process continues, depending on the initial preform temperature, two significantly different behaviors are possible. For the preform preheated above the metal melting point (933 K, for aluminum), heat conduction progressively smooths the temperature gradient to a point that the transition between composite (metal and fibers) and preform (fibers and inert gas) becomes indistinguishable (it has been indicated by an arrow in Figure 2(a)). When the preform preheating temperature is below the metal melting point, on the other hand, the temperature of the melt decreases until it reaches its melting temperature, at which point partial solidification characterized by a constant-temperature two-phase zone (*cf.* Figure 2(a)) can be observed. Two regions are clearly distinguishable upstream and downstream from the infiltration front, which now can be clearly identified by a steep temperature gradient separating the metal infiltrated composite from the preform. As the infiltration progresses through the preform, the two-phase zone expands,

with its two boundaries, from here on referred to as the “remelting” and “infiltration” fronts, exhibiting their own dynamics (*cf.* Figure 2(b)).

A comprehensive analysis of the process has been carried out by Mortensen *et al.*<sup>[4]</sup> Their approach was to simplify the governing equations for limiting conditions. The equations thus simplified were solved in an analogous manner to similarity solutions of moving fronts. The similarity variable was defined by Mortensen as

$$\chi = \frac{x}{\psi\sqrt{t}} \quad [11]$$

where  $x$  and  $t$  represent the space and time variables, and  $R$  is a scaling factor. The scaling factor is chosen such as the similarity variable is unitary at the infiltration front (*i.e.*,  $\chi = 1$  for  $x = L_f$ , where  $L_f$  is the axial location of the infiltration front). Using this transformation, a closed form solution of the governing equations, which showed satisfactory agreement with experimental results, was obtained.<sup>[5]</sup> The infiltration dynamics could then be described by the scaling factor,  $\psi$ , as

$$\psi = \begin{cases} \sqrt{\frac{2\kappa\Delta P}{\mu\varepsilon}} & \text{in the absence of solidification} \\ \sqrt{\frac{2\Delta P}{\mu\varepsilon\left(\frac{\chi_s}{\kappa} + \frac{1-\chi_s}{\kappa'}\right)}} & \text{in the presence of solidification} \end{cases} \quad [12]$$

where  $\Delta P$  is the pressure drop across the liquid column,  $\kappa$  is the permeability of the uninfiltreated preform,  $\mu$  is the dynamic viscosity of the melt, and  $\varepsilon$  is the void fraction in the uninfiltreated preform. Two additional variables are introduced for the case of solidification:  $\kappa'$ , the permeability of the two-phase zone; and  $\chi_s$ , the location of the remelting front relative to the infiltration length (*i.e.*, the two-phase zone length relative to the infiltration length would be  $1 - \chi_s$ ). These equations, together with the flow description, Eq. [3], and the analytical expressions for the temperature profile, the length of the two-phase zone, and the solid fraction in the two-phase zone, describe the dynamics of the infiltration process. The approach, however, relies on the hypothesis that the infiltration process can be described as a constant-pattern process with a two-phase zone with constant solid fraction and length relative to the infiltration length (*i.e.*,  $\varepsilon_s$  and  $\chi_s$  are assumed to depend only on physical properties and remain constant throughout the process). The comparison between the analytical predictions outlined previously and the numerical results, presented next, shows that  $\varepsilon_s$  and  $\chi_s$  do not remain constant during infiltration.

#### A. Unidirectional Infiltration in the Absence of Solidification

When the initial preform temperature is sufficiently high (or when the infiltration velocity is high), no solidification of the matrix will occur. The permeability in the composite will then remain constant. This simple case is considered first in order to compare the present results with the analytical model presented by Mortensen *et al.*<sup>[4]</sup> The infiltra-

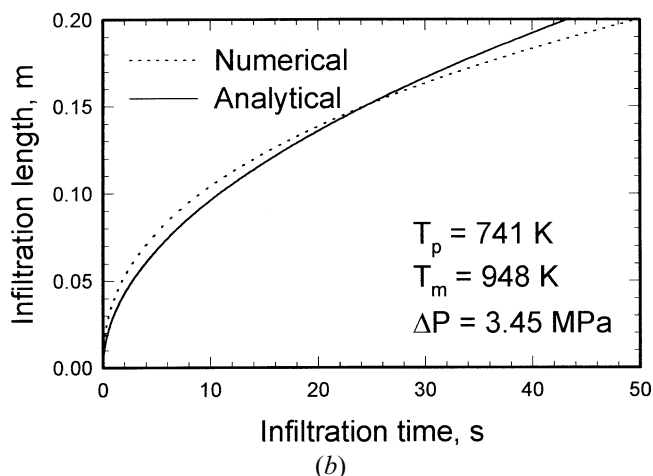
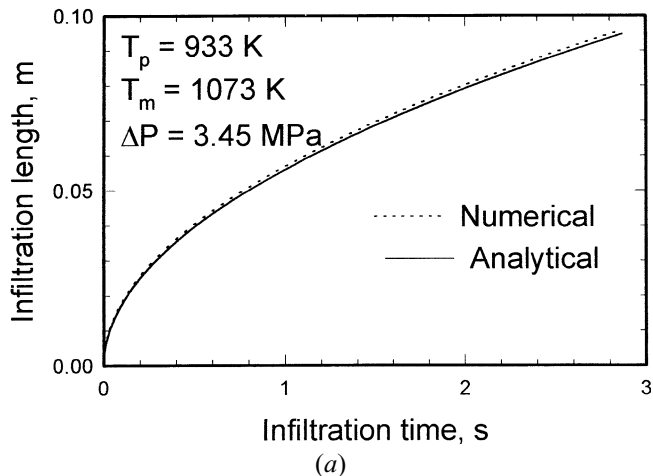


Fig. 3—Comparison of infiltration dynamics predicted analytically (solid line) and numerically (dashed line) in the (a) absence of solidification and (b) with partial solidification.

tion dynamics are shown in Figure 3(a). The satisfactory agreement existing between the numerical and analytical predictions validates the numerical model. This agreement can be easily anticipated: the only hypothesis of the similarity solution that is not verified in this situation is the constant pressure drop across the infiltrated preform. Indeed, the hydrostatic correction will decrease the driving force and, therefore, the infiltration velocity. This effect, as well as end effects, appears negligible, nevertheless.

#### B. Unidirectional Infiltration in the Presence of Solidification

Numerical predictions can also be compared with the experimental and analytical results for unidirectional adiabatic infiltration with solidification. When the initial fiber preform temperature and the initial metal temperature (or the infiltration velocity) are not sufficiently high as to avoid solidification, solid metal will form upstream from the infiltration front as a coating surrounding the packing fibers. The remaining liquid will flow further downstream, encountering a new set of cold fibers, where additional solidification will take place in an analogous manner. Upstream from the infiltration front, wherever solid and liquid metal coexist, the temperature remains uniform at the metal melt-

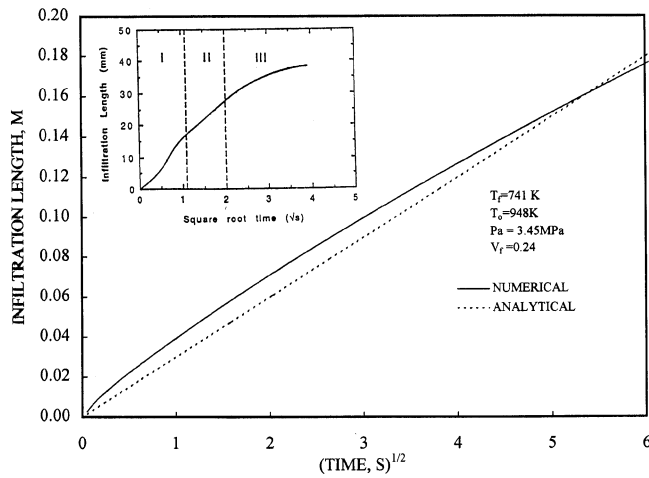


Fig. 4—Linearized plot of the infiltration dynamics as predicted (a) analytically and (b) numerically. Inset shows experimental infiltration dynamics (adapted from Masur *et al.*<sup>[5]</sup>).

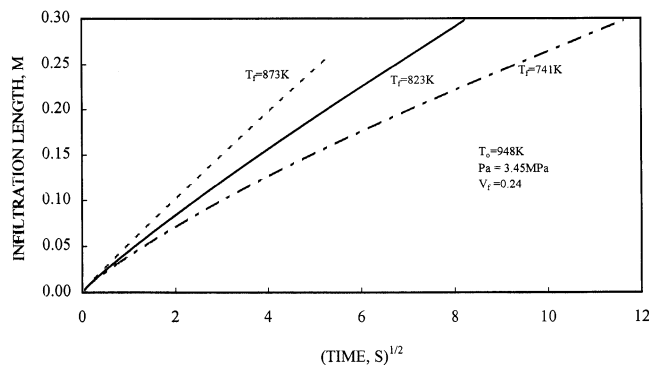


Fig. 5—Infiltration dynamics for different preform temperatures.

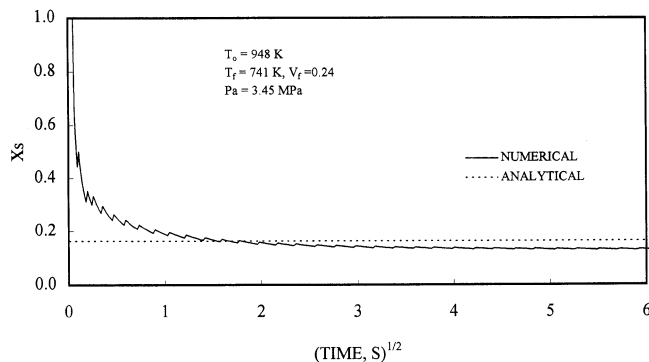


Fig. 6—Dynamics of the remelting front as predicted analytically (dashed line) and numerically (solid line).

ing temperature. At some point (*i.e.*, at the remelting front), remelting of the metal occurs due to the influx of a superheated liquid metal at the preform entrance. The composite is then comprised of two zones: a zone where solid and liquid metal coexist, extending from the infiltration front to the remelting front; and a zone where the metal is entirely liquid and covers the rest of the composite. Masur *et al.*<sup>[5]</sup> reported a satisfactory agreement between their analytical solution and experimental results. When the analytical results are compared with the numerical model for the same conditions (*cf.* Figure 3b), some discrepancies are clearly

noticeable. The analytical model underpredicts the infiltration length initially and overpredicts it at longer times.

These discrepancies can be explained as follows: to find the scaling factor  $R$  in the similarity variable,  $\chi$ , Masur *et al.*<sup>[5]</sup> measured the slopes of plots of the experimental infiltration length as a function of the square root of the infiltration time. Since the plots were nonlinear, the parameter  $\psi$  was determined from a selected section of the plot (*i.e.*, section “II” in the inset of Figure 4), arbitrarily defined as that corresponding to “before sufficient solidification occurred.” The agreement between the analytical predictions and experiments, therefore, does not correspond to the entire infiltration process but only to a fraction of it. The numerical results (*cf.* Figure 4) show a nonlinear trend, which deviates from the analytical results. The nonlinearity, very pronounced at the low preform temperatures, disappears as the preform temperature is increased (*cf.* Figure 5). This suggests that the solidification of the metal is the main cause for the differences between the analytical and numerical results. The deviation from linearity, however, appears to be consistent with the experimental data. Since a linear correlation is the basis for the analytical solution, discrepancies are to be expected. The numerical model, however, yields the following additional results: (1) dynamics of the remelting front; (2) dynamics of the solid fraction distribution; and (3) effect of process variables on the microstructure, which lend it more credibility than its analytical counterpart.

#### 1. Dynamics of the remelting front

In the analytical model, the ratio of the remelting front position to the infiltration front position,  $\chi_s$ , is assumed constant for the given process conditions. This assumption implies that the infiltration process can be characterized as a constant-pattern propagation one. This parameter was investigated numerically for different preform temperatures. These results (*cf.* Figure 6) show that the remelting and the infiltration fronts are initially at the same position (*i.e.*,  $\chi_s = 1$ ). As the melt infiltrates and solidification starts, a two-phase zone emerges and starts expanding: *i.e.*, the value of  $\chi_s$  decreases. Because of the finite nature of the preform, the length of the two-phase zone, relative to the infiltration length, will never reach a steady-state value. The process shows a quasiasymptotic value for  $\chi_s$ , which would suggest that end effects are only minor.

Figure 6 shows that  $\chi_s$  will coincide with the analytical value<sup>[4]</sup> at about 4 seconds into the infiltration process: the two-phase zone is shorter than the analytical value before this time and longer than the analytical prediction afterward. For the experimental conditions illustrated, the analytical prediction corresponds to a value of  $\chi_s = 0.163$ , while the numerical prediction of  $\chi_s$  shows an asymptotic trend toward 0.14. Therefore, the simplified model will underestimate the infiltration velocity before the first 4 seconds of infiltration and overestimate it at later times. The impact of this deficiency of the simplified model on its predictive ability will depend, therefore, on the dimensions of the preform being infiltrated. For instance, Masur *et al.*<sup>[5]</sup> presented comparisons for infiltration lengths in the range of 4 to 5 cm, which would occur in the first 2 to 3 seconds of infiltration. As discussed previously, the underestimation of the infiltration velocity can be quite significant during such short times (*i.e.*, the initial infiltration transients would



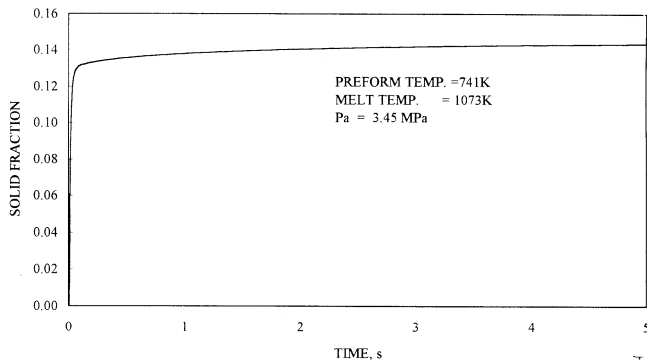


Fig. 7—Dynamics of the solid fraction at the infiltration front.

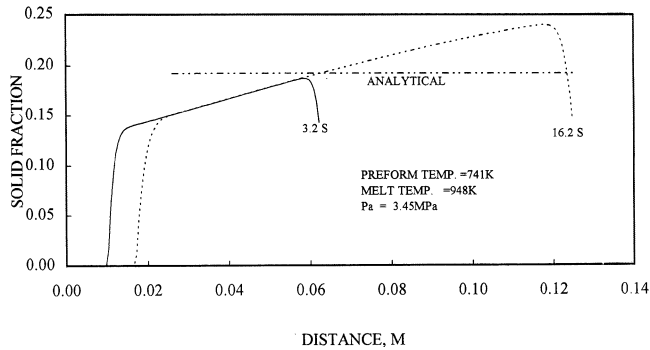


Fig. 8—Solid fraction distribution as predicted analytically (dashed line) and numerically.

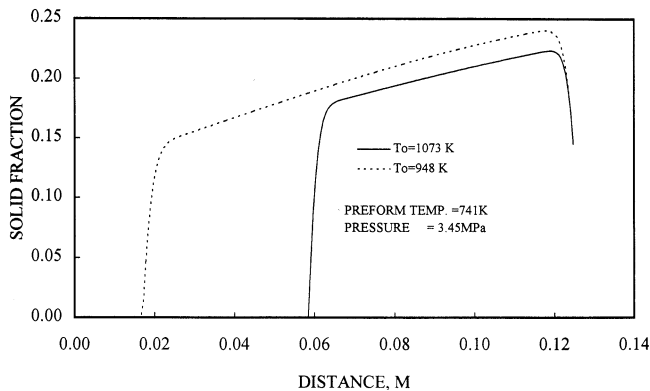


Fig. 9—Effect of the superheating on the solid fraction distribution.

not have disappeared during the first few seconds of infiltration).

### 2. Dynamics of the solid fraction distribution

While the solid fraction at the infiltration front (*cf.* Figure 7) reaches a constant value very rapidly, it is not constant in the two-phase zone, as shown in Figure 8 for two typical infiltration times. The analytical model, on the other hand, assumes a constant solid fraction value for the two-phase zone. For the process conditions illustrated, the numerical result is approximately a solid fraction of 14 pct at the infiltration front against an analytically predicted constant solid fraction of 19.2 pct. If the dynamics of the solid fraction are investigated in more detail, one can observe that during the early stages ( $\sim 3$  seconds) of infiltration, the maximum solid fraction is lower than the

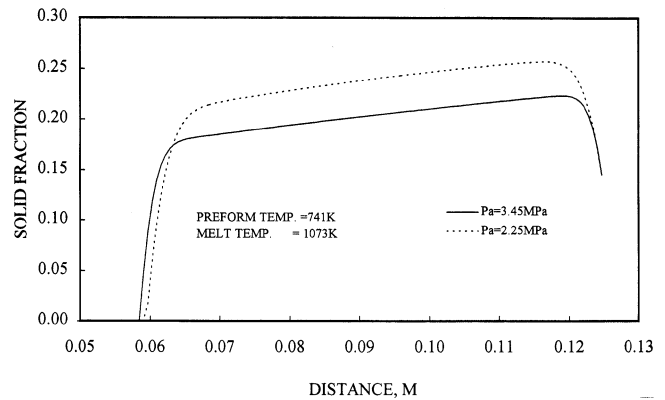


Fig. 10—Effect of the applied pressure on the solid fraction distribution.

analytical prediction. As infiltration continues, the maximum solid fraction exceeds the analytical prediction. During this second stage, the average solid fraction will approximately correspond with the constant value predicted by the simplified model. However, because of the initial lower solid fraction, the permeability of the preform will be underestimated during the infiltration of the first 6 cm. This will, in turn, result in an underestimation of the infiltration rate. Similarly, at the later stages of the infiltration process, when sufficient solid has formed, and the maximum and the average solid fractions are higher than those predicted analytically, the analytical model will overestimate the overall permeability of the preform, as well as the infiltration rate.

### 3. Effect of process parameters on the solid fraction distribution

The effect of the degree of melt superheating on the solid fraction distribution along the specimen length is illustrated in Figure 9. This figure shows the solid fraction distribution, for identical infiltration lengths, for different degrees of superheating. The initial preform temperature, total applied pressure, and fiber volume fraction were kept constant for two melt temperatures: 1073 and 948 K. This figure shows that the length of the two-phase zone and the average solid fraction in this zone decrease with increasing superheating. In other words, the extent of superheating will affect not only the remelting front position but also the solid fraction distribution in the two-phase zone.

A similar investigation was carried out on the effect of the applied pressure on the solid fraction distribution. The initial preform and melt temperatures, as well as the fiber volume fraction, were kept constant for the comparison shown in Figure 10. This figure presents the solid fraction distribution for different applied pressures, for the same infiltration length. The results show that the applied pressure does not significantly influence the remelting front position, but it considerably affects the solid fraction distribution. At higher pressure, because of the faster superficial velocity, the solid fraction in the two-phase zone is significantly lower than that observed at the lower pressure. However, only a minor increase in the length of the two-phase zone occurs. The analytical model, on the other hand, does not account for the effects of the degree of superheating or the applied pressure on the solid fraction distribution. The solid fraction distribution is a very important parameter, which

will influence the microstructure and the micro/macro-segregation of solutes during pressure infiltration casting of metallic alloys.

## V. CONCLUSIONS

A mathematical model for the dynamics of pressure infiltration processes has been formulated and solved numerically. The numerical solution is reliable and robust and can account for end effects and structural dynamics. The numerical solution is compared against a classical similarity solution. Both models are in agreement for the homogeneous infiltration in the absence of phase-change effects, where end effects appeared negligible and the assumption of constant-pattern propagation was valid. For conditions that result in partial solidification (and, eventually, subsequent plugging), the numerical and analytical solutions differ substantially. Most of the discrepancies are caused by the assumption of a constant-pattern propagation made in the similarity solution. Actual infiltration processes never show constant pattern propagation. The numerical solution shows the presence of significant end effects and an unsteady mode of propagation, in contrast to the uniform solid fraction and constant ratio between the infiltration and remelting fronts, as assumed by the analytical solution. Although the overall infiltration dynamics are not significantly affected by these differences, the related issues such as 2-D effects, segregation, and alloy infiltration can be expected to be markedly influenced.

Summarizing, the numerical analysis, presented previously, leads to the following conclusions.

1. End effects might become preponderant during the initial and final stages of the infiltration, diminishing the value of asymptotic analyses as reliable design tools and rendering them only useful indicative tools.
2. Although heat conduction in the preform might be negligible in estimating the temperature profile, it cannot be neglected when the matrix and the preform have similar conductivities. The steep thermal gradients existing downstream from the solidifying front may combine with low thermal conductivities to significantly influence the infiltration dynamics.
3. The two-phase zone dynamics are very sensitive to the occurrence of partial solidification.
4. The effect of the degree of superheating on the infiltration dynamics is not as significant as that of the preform temperature. The degree of superheating, however, affects the length of the two-phase zone and the solid fraction distribution.
5. The applied pressure has a negligible effect on the length of the two-phase zone, but it influences the solid fraction distribution substantially.

## ACKNOWLEDGMENTS

Support provided by the Processing Science and Technology Branch, NASA-Lewis Research Center (Cleveland, OH), is gratefully acknowledged. The authors are also thankful to the reviewers for their careful reading and valuable suggestions.

## REFERENCES

1. S. Nagata and K. Matsuda: *Trans. Jpn. Foundrymen's Soc.*, 1982, vol. 2, pp. 616-20.
2. G.P. Martins, D.L. Olson, and G.R. Edwards: *Metall. Trans. B*, 1988, vol. 19B, pp. 95-101.
3. F.A. Giroto, R. Fedon, J.M. Quenisset, and R. Naslain: *J. Reinforced Plastics Composites*, 1990, vol. 9, pp. 456-69.
4. A. Mortensen, L.J. Masur, J.A. Cornie, and M.C. Flemings: *Metall. Trans. A*, 1989, vol. 20A, pp. 2535-47.
5. L.J. Masur, A. Mortensen, J.A. Cornie, and M.C. Flemings: *Metall. Trans. A*, 1989, vol. 20A, pp. 2549-57.
6. A. Mortensen and V. Michaud: *Metall. Trans. A*, 1990, vol. 21A, pp. 2059-72.
7. R.B. Calhoun and A. Mortensen: *Metall. Trans. A*, 1992, vol. 23A, pp. 2291-99.
8. E. Lacoste, M. Aboulfatah, M. Danis, and F. Giroto: *Metall. Trans. A*, 1993, vol. 24A, pp. 2667-78.
9. Kwan-Hong Shin: Ph.D. Thesis, The University of Iowa, Iowa City, IA, 1993.
10. S. Long, Z. Zhang, and H.M. Flower: *Acta Metall. Mater.*, 1994, vol. 42 (4), pp. 1389-97.
11. T. Yamauchi and Y. Nishida: *Acta Metall. Mater.*, 1995, vol. 43 (4), pp. 1313-21.
12. D.B. Spalding: in *Computer Simulation for Fluid, Heat and Mass Transfer in Reciprocation Engines*, Hemisphere Publishing Corp., New York, NY, 1989, [pp. 383-455.]
13. D. Vortmeyer, K.J. Dietrich, and K.O. Ring: *Adv. Chem. Ser.*, 1974, vol. 133, pp. 588-99.
14. J.E. Gatica, H.J. Viljoen, and V. Hlavacek: *Chem. Eng. Sci.*, 1989, vol. 44 (9), pp. 1853-70.
15. J.M. Straus: *J. Fluid Mech.*, 1974, vol. 64 (1), pp. 51-63.
16. P.V. Danckwerts: *Chem. Eng. Sci.*, 1953, vol. 2 (1), pp. 1-18.
17. A.S. Sangani and A. Acrivos: *Int. J. Multiphase Flow*, 1982, vol. 8, pp. 193-206.
18. J.E. Drummond and M.I. Tahir: *Int. J. Multiphase Flow*, 1984, vol. 10, pp. 515-40.
19. S.K. Datta, N. Simhai, S.N. Tewari, J.E. Gatica, and M. Singh: *Metall. Mater. Trans. A*, 1996, vol. 27A, pp. 3669-74.
20. A. Mortensen and I. Jin: *Int. Mater. Rev.*, 1992, vol. 37 (3), pp. 101-28.
21. D. Longworth: in *Moving Boundary Problems in Heat Flow and Diffusion*, J.R. Ockendon and W.R. Hodgkin, eds., Clarendon Press, Oxford, United Kingdom, 1975.
22. V.R. Voller and M. Cross: *Int. J. Heat Transfer*, 1981, vol. 24, pp. 5454-56.
23. V.R. Voller, M. Cross, and N.C. Markatas: *Int. J. Num. Methods Eng.*, 1987, vol. 24, pp. 271-84.
24. J.E. Gatica, P.A. Dimitriou, J.A. Puszyński, and V. Hlavacek: *Int. J. SHS*, 1995, vol. 4 (2), pp. 123-36.
25. G.R. Cappleman, J.F. Watts, and T.W. Clyne: *J. Mater. Sci.*, 1985, vol. 20, pp. 2159-68.